Article ID: 1006-8775(2012) 03-0369-08

SENSITIVITY OF PRECIPITATION TO SEA SURFACE TEMPERATURE AND ITS DIURNAL VARIATION: A PARTITIONING ANALYSIS BASED ON SURFACE RAINFALL BUDGET

ZHOU Yu-shu (周玉淑)[1], Xiao-fan LI (李小凡)[2]

(1. Laboratory of Cloud-Precipitation Physics and Severe Storms (LACS), Institute of Atmospheric Physics, Chinese Academy of Sciences, Beijing 100029 China; 2. NOAA/NESDIS/Centre for Satellite Applications and Research, Camp Springs, Maryland, USA)

Abstract: The sensitivity of precipitation to sea surface temperature (SST) and its diurnal variation is investigated through a rainfall partitioning analysis of two-dimensional cloud-resolving model experiments based on surface rainfall budget. For all experiments, the model is set up using zero vertical velocity and a constant zonal wind and is integrated over 40 days to reach quasi-equilibrium states. The 10-day equilibrium grid-scale simulation data and a time-invariant SST of 29°C are used in the control experiment. In the sensitivity experiments, time-invariant SSTs are 27°C and 31°C with an average value of 29°C when the minimum and maximum values of diurnal SST differences are 1°C and 2°C, respectively. The results show that the largest contribution to total rainfall is from the rainfall with water vapor convergence and local atmospheric drying and hydrometeor gain/divergence (~30%) in all experiments. When SST increases from 27°C to 29°C, the contribution from water vapor convergence decreases. The increase of SST reduces the contribution of the rainfall with water vapor convergence primarily through the decreased contribution of the rainfall with local atmospheric drying and hydrometeor gain/divergence and the rainfall with local atmospheric moistening and hydrometeor loss/convergence. The inclusion of diurnal variation of SST with the diurnal difference of 1°C decreases the rainfall contribution from water vapor convergence primarily through the decreased contribution of the rainfall with local atmospheric moistening and hydrometeor loss/convergence. The contribution of the rainfall from water vapor convergence is barely changed as the diurnal difference of SST increases from 1°C to 2°C.

Key words: precipitation statistics; sea surface temperature (SST); diurnal variation; equilibrium cloud-resolving model simulation

CLC number: P435 **Document code:** A

1 INTRODUCTION

Sea surface temperature (SST) has important impacts on precipitation. Lau et al.[1] found 22% increase in convective precipitation and 13% increase in surface evaporation rate are associated with imposed SST increases from 28°C to 30°C in the experiments imposed by the same large-scale forcing. Costa et al.[2] revealed that 6.4% increase in precipitation is associated with 2°C increase of SST, which results from large offset between 17.8% increase in convective precipitation and 19.0% decrease in stratiform precipitation. Wu and Moncrieff[3] showed 3.3% and 5.8% increases in time-mean precipitation as time-mean SST increases, respectively, from 27.4°C to 29.4°C and from 29.4°C to 31.4°C. Cui and Li[4] found that the increase of SST from 29°C to 31°C leads to a 19 % increase of surface rain rate in the equilibrium cloud-resolving model simulations imposed by zero large-scale vertical velocity. Recently, Zhou and Li[5] analyzed equilibrium cloud-resolving model simulation data from Gao et al.[6] (the same data used in this study) with the surface rainfall equation proposed by Gao et al.[7]. They studied the sensitivity of precipitation to SST and revealed that the increase in surface evaporation over clear sky regions associated with the increase in SST from 29°C to 31°C intensifies the water vapor transport to convective regions that enhances the convective and mean rainfall. The

Received 2010-12-20; **Revised** 2012-05-09; **Accepted** 2012-07-15

Foundation item: State Key Development Program for Basic Research of China (2009CB421505); Projects of the Natural Science Foundation of China (41075044; 41075079)

Biography: ZHOU Yu-shu, Ph.D., primarily undertaking mesoscale dynamical diagnosis and numerical modeling analyses.

Corresponding author: ZHOU Yu-shu, e-mail: zys@mail.iap.ac.cn

increase in mean surface rainfall is related to the mean local atmospheric drying and decrease of mean hydrometeor concentration when the diurnal variation of SST is included in the model.

Most of previous studies focus on area-mean surface rainfall, which may contain the rainfall resulting from different processes as revealed by the surface rainfall equation from Gao et al.[7] and the rainfall from convective and raining stratiform regions. Shen et al.[8] proposed a new rainfall separation scheme based on surface rainfall budget to categorize grid rainfall model simulation data during Tropical Ocean Global Atmosphere Coupled Ocean Atmosphere Response Experiment (TOGA COARE) into eight rainfall types. They showed that the rainfall type with water vapor divergence and local atmospheric drying and hydrometeor loss/convergence has the largest contribution to total rainfall. The objective of this research is to study the sensitivity of precipitation to SST and its diurnal variation using the new rainfall separation scheme. Shen et al.[8] further compared the results using the new rainfall separation scheme with the results using a convective-stratiform rainfall separation scheme from previous study and found that about 30% of convective rainfall is associated with water vapor divergence, which is contradictory to the fact that convective rainfall is usually associated with water vapor convergence. Thus, the results from previous study[5] will be compared with the results from the calculations from the current study. The model, simulation data, and surface rainfall equation are briefly discussed in the next section. The results are presented in section 3. The summary is given in section 4.

2 MODEL, EXPERIMENT, AND SURFACE RAINFALL EQUATION

The data analyzed in this study come from two-dimensional equilibrium sensitivity cloud-resolving model simulation by Gao et al.[6]. The model was developed by Soong and Ogura[9], Soong and Tao[10], and Tao and Simpson[11] and further modified by Sui et al.[12] and Li et al.[13]. The model includes prognostic equations for mixing ratios of five cloud species (including cloud water, raindrop, cloud ice, snow, and graupel), cloud microphysical parameterization schemes[14-18], and interactive solar and thermal infrared radiation parameterization schemes[19-20]. The model uses cyclic lateral boundary, a horizontal domain of 768 km, a horizontal grid resolution of 1.5 km, 33 levels in the vertical, and a time step of 12 s. The top model level is 42 hPa. The vertical grid resolution ranges from about 200 m near the surface to about 1 km near 100 hPa. The detailed model description can be found in Gao and Li[21].

Experiments SST29, SST27 and SST31 are forced by time-invariant SSTs of 29°, 27° and 31°C, respectively. Experiments SST29D1 and SST29D2 have diurnally-varying SSTs with a time mean of 29°C and diurnal difference of 1° and 2°C, respectively [also see Figure 1 in Gao et al.[6]]. SST reaches maximum and minimum respectively at hours 16 and 7. The model is forced by the zero zonally-uniform large-scale vertical velocity and a time-invariant and vertically-uniform zonal wind of 4 m s^{-1}, and is integrated to quasi-equilibrium rates within 40.5 days in all five experiments. The vertical profiles of temperature and specific humidity observed at 0400 LST 19 December 1992 from Sui et al.[22] during TOGA COARE[22] are used as the initial conditions. The two-dimensional cloud-resolving model has been used to study precipitation processes associated with tropical convection during TOGA COARE and South China Sea Monsoon Experiment (SCSMEX) and the landfall of tropical storms and pre-summer heavy rainfall[23-33].

Following Gao et al.[7] and Zhou et al.[34], the surface rainfall equation can be expressed by

$$P_s = Q_{WVT} + Q_{WVF} + Q_{WVE} + Q_{CM}, \quad (1)$$

$$Q_{WVT} = -\frac{\partial [q_v]}{\partial t}, \quad (1a)$$

$$Q_{WVF} = -[\bar{u}^o \frac{\partial \bar{q}_v}{\partial x}] - [\frac{\partial (u' q_v')}{\partial x}] - [\bar{u}^o \frac{\partial q_v'}{\partial x}] - [w' \frac{\partial \bar{q}_v}{\partial z}], \quad (1b)$$

$$Q_{WVE} = E_s, \quad (1c)$$

$$Q_{CM} = Q_{CMC} + Q_{CMR} + Q_{CMI} + Q_{CMS} + Q_{CMG}, \quad (1d)$$

$$Q_{CMC} = -\frac{\partial [q_c]}{\partial t} - [\frac{\partial}{\partial x}(\bar{u}^o + u')q_c], \quad (1e)$$

$$Q_{CMR} = -\frac{\partial [q_r]}{\partial t} - [\frac{\partial}{\partial x}(\bar{u}^o + u')q_r], \quad (1f)$$

$$Q_{CMI} = -\frac{\partial [q_i]}{\partial t} - [\frac{\partial}{\partial x}(\bar{u}^o + u')q_i], \quad (1g)$$

$$Q_{CMS} = -\frac{\partial [q_s]}{\partial t} - [\frac{\partial}{\partial x}(\bar{u}^o + u')q_s], \quad (1h)$$

$$Q_{CMG} = -\frac{\partial [q_g]}{\partial t} - [\frac{\partial}{\partial x}(\bar{u}^o + u')q_g], \quad (1i)$$

where u and w are zonal and vertical air wind components, respectively; q_v is specific humidity; $q_5 = q_c + q_r + q_i + q_s + q_g$, q_c, q_r, q_i, q_s, q_g are the mixing ratios of cloud water, raindrops, cloud ice, snow, and graupel, respectively; E_s is surface evaporation; the prime denotes a perturbation from the model domain mean (over bar); and the symbol ° is an imposed forcing. The surface rain rate is determined by local vapor storage (Q_{WVT}), water vapor convergence (Q_{WVF}), surface evaporation (Q_{WVE}), and hydrometeor convergence minus storage (Q_{CM}) from cloud water (Q_{CMC}), rain (Q_{CMR}), cloud ice (Q_{CMI}), snow (Q_{CMS}), and graupel (Q_{CMG}). The surface rainfall processes Q_{WVT}, Q_{WVF}, and Q_{CM} could be positive or negative. Following Shen et al.[8], T and t represent local atmospheric drying (Q_{WVT} >0) and moistening (Q_{WVT} <0), respectively. F and f denote water vapor convergence (Q_{WVF} >0) and divergence (Q_{WVF} <0), respectively. M and m represent hydrometeor loss/convergence (Q_{CM} >0) and hydrometeor gain/divergence (Q_{CM} <0), respectively. Thus, eight rainfall types (TFM, TFm, tFM, tFm, TfM, Tfm, tfM, tfm) will be categorized using the grid simulation data based on different signs of Q_{WVF}, Q_{WVT}, and Q_{CM}, and will be analyzed in this study (see the summary of rainfall types in Table 1). The rainfall type tfm will not be discussed in this study because it does not contribute to total rainfall.

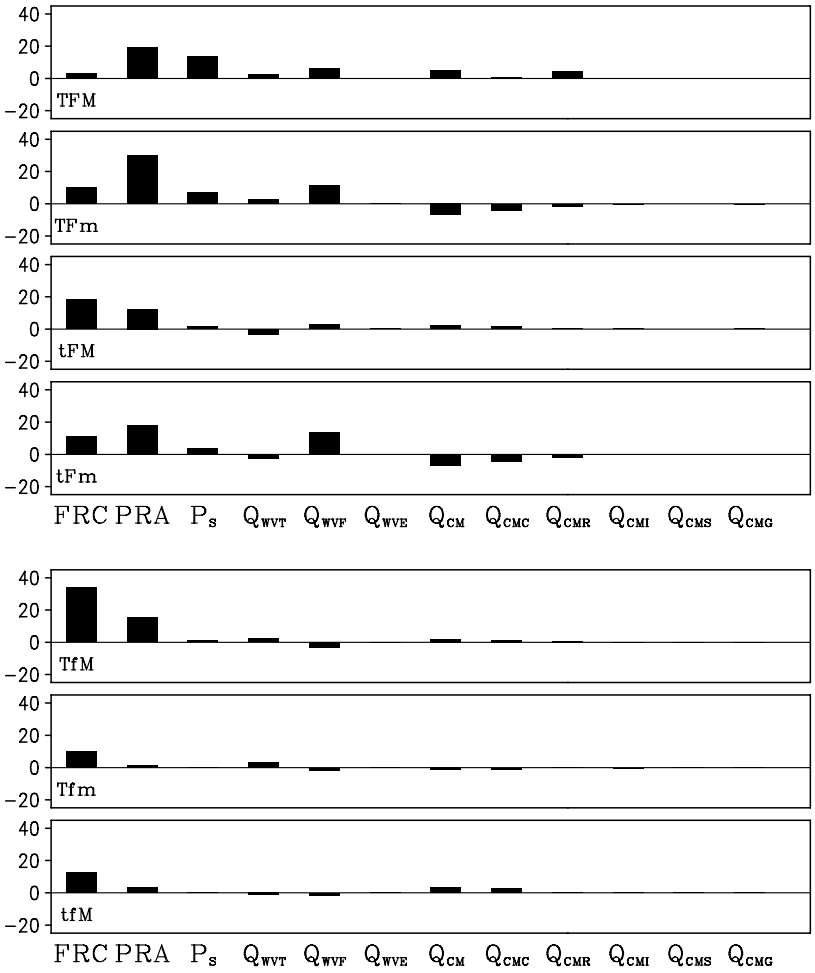

Figure 1. Fractional rainfall coverage (FRC) and percentage of rain amount over total rainfall amount (PRA), and means of P_S, Q_{WVT}, Q_{WVF}, Q_{WVE}, Q_{CM}, Q_{CMC}, Q_{CMR}, Q_{CMI}, Q_{CMS}, and Q_{CMG} of TFM, TFm, tFM, and tFm, TfM, Tfm, and tfM in SST29. Units are mm h^{-1} for P_S, Q_{WVT}, Q_{WVF}, Q_{WVE}, and Q_{CM}, and % for FRC and PRA.

Table 1. Summary of rainfall types. T and t represent local atmospheric drying and moistening, respectively. F and f represent water vapor convergence and divergence, respectively. M and m represent hydrometeor loss/convergence and gain/divergence, respectively.

Type	Description
TFM	Water vapor convergence, local atmospheric drying, and hydrometeor loss/convergence
TFm	Water vapor convergence, local atmospheric drying, and hydrometeor gain/divergence
tFM	Water vapor convergence, local atmospheric moistening, and hydrometeor loss/convergence
tFm	Water vapor convergence, local atmospheric moistening, and hydrometeor gain/divergence
TfM	Water vapor divergence, local atmospheric drying, and hydrometeor loss/convergence
Tfm	Water vapor divergence, local atmospheric drying, and hydrometeor gain/divergence
tfM	Water vapor divergence, local atmospheric moistening, and hydrometeor loss/convergence
tfm	Water vapor divergence, local atmospheric moistening, and hydrometeor gain/divergence; this rainfall type has no contribution to total rainfall in this study

3 RESULTS

Table 2 presents an analysis of percentage of rainfall amount from each rainfall type over total rainfall amount (PRA), which shows that the rainfall (TFm) with water vapor convergence and local atmospheric drying and hydrometeor gain/divergence is the largest contributor (30.2%) to total rainfall in SST29 (Figure 1), while Shen et al[8] found that the rainfall type TfM with water vapor divergence and local atmospheric drying and hydrometeor loss/convergence has the largest contribution (30.8%) to total rainfall in their simulation imposed by non-zero COARE forcing. TFm is the fourth largest rainfall contributor in SST29 in this study. While SST29 and COARE simulation show similar fractional rainfall coverage for TfM (FRC; ~35%), the mean surface rain rate of TfM is much lower in SST29 (1.10 mm h^{-1}) than in COARE simulation (2.82 mm h^{-1}); this appears to be from weaker hydrometer loss/convergence of water and graupel clouds in SST29 (2.13 mm h^{-1}) than in COARE simulation (4.67 mm h^{-1}). FRC of TFm is larger in SST29 (10.1%) than in COARE simulation (6.9%), whereas the rain rate of TFm is lower in SST29 (7.18 mm h^{-1}) than in COARE simulation (8.27 mm h^{-1}). Thus, the expansion of rainfall coverage for TFm in SST29 and reduction of the rain rate in COARE simulation are responsible for the switch of the largest contributor to total rainfall from TfM in COARE simulation to TFm. The largest rainfall contributor from different rainfall types in SST29 and COARE simulation indicates that the large-scale forcing plays an important role in determining the largest rainfall contributor.

Table 2. Percentages of rain amount over total rainfall amount (PRA) for the rainfall with water vapor convergence (TFM+TFm+tFM+tFm) in this study and convective rainfall in Zhou and Li (2009) in five sensitivity experiments. Units: %.

	SST29	SST27	SST31	SST29D1	SST29D2
TFM+TFm+tFM+tFm	80.21	79.83	77.60	77.10	76.99
Convective rainfall	56.92	54.62	61.64	60.27	61.33

Although the rainfall type TFM in SST29 has the smallest rainfall coverage (3.4%), it has the highest rain rate (13.92 mm h^{-1}) because all rainfall processes favor rainfall. As a result, TFM is the second largest rainfall contributor (19.4%). The largest water vapor convergence occurs in tFm in SST29, but the local atmospheric moistening and hydrometeor gain/divergence largely offset the water vapor convergence, resulting in moderate rain rate for the third largest rainfall contributor. 80.2% of total rainfall comes from the four rainfall types with water vapor convergence in SST29. Tfm and tfM have negligibly small contributions to total rainfall.

The increase of SST leads to an increase of rainfall contribution by water vapor convergence (TFM+TFm+tFM+tFm) from 79.8% in SST27 to 80.2% in SST29, but a decrease from 80.2% in SST29 to 77.6% in SST31. The increase of SST from 27°C in SST27 to 29°C in SST29 leads to the increases of PRA for TFm and tFM, whereas the increase of SST from 29°C in SST29 to 31°C in SST31 results in the decreases of PRA for TFm and tFM (Figure 2). When the SST increases from 27°C to 29°C, the largest increase of PRA occurs in TFm, which is from 27.5% in SST27 to 30.2% in SST29. Although both experiments show similar rainfall coverage (10.1%), the rain rate is much higher in SST29 (7.18 mm h^{-1}) than in SST27 (4.94 mm h^{-1}). Thus, the increase of PRA for TFm is associated with the increase of rain rate, which comes primarily from the increase in water vapor convergence. The moderate increase of PRA for tFM results from the enhanced rainfall through the

increase in water vapor convergence and cloud water hydrometeor loss/convergence. When the SST increases from 29°C to 31°C, the rainfall contribution of TFm and tFM is reduced through the shrink of rainfall convergence. The rainfall contribution of TfM is increased when the SST increases from 27°C to 31°C, but the increase of PRA is much larger when the SST increases from 29°C to 31°C than when the SST increases from 27°C to 29°C. The enhanced PRA of TfM results from the expanded rainfall coverage and intensified rainfall through the increase in local atmospheric drying and water hydrometeor loss/convergence.

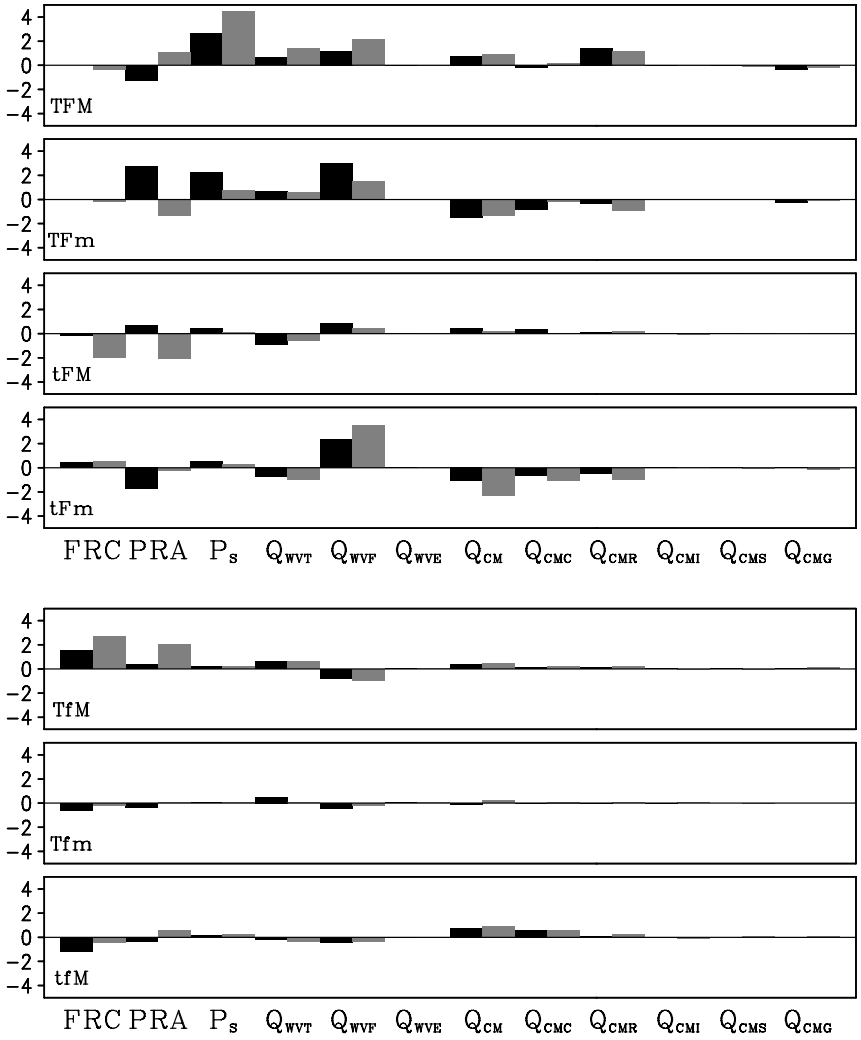

Figure 2. Fractional rainfall coverage (FRC) and percentage of rain amount over total rainfall amount (PRA), and means of P_S, Q_{WVT}, Q_{WVF}, Q_{WVE}, Q_{CM}, Q_{CMC}, Q_{CMR}, Q_{CMI}, Q_{CMS}, and Q_{CMG} of TFM, TFm, tFM, and tFm, TfM, Tfm, and tfM for SST29-SST27 (black) and SST31-SST29 (grey). Units are mm h^{-1} for P_S, Q_{WVT}, Q_{WVF}, Q_{WVE}, and Q_{CM} and % for FRC and PRA.

The inclusion of diurnal variation of SST with the diurnal difference of 1°C in the model simulation decreases the rainfall contribution of the rainfall with water vapor convergence from 80.2% in SST29 to 77.1% in SST29D1. When the diurnal difference of SST imposed in the model increases from 1°C to 2°C, the rainfall contribution of the rainfall with water vapor convergence is barely changed (77.1% in SST29D1 and 77.0% in SST29D2). The inclusion of diurnal variation of SST with the diurnal difference of 1°C in the model simulation in SST29D1 decreases the rainfall contribution of TFm and tFM (Figure 3). The reduction in rainfall contribution of TFm comes from the shrink of rainfall coverage whereas the reduced rainfall contribution of tFM results from the shrink of rainfall coverage as well as the weakened surface rainfall caused by the decreases in local atmospheric drying and cloud water hydrometeor loss/convergence. When the diurnal difference of imposed diurnal variation of SST increases from 1°C

in SST29D1 to 2°C in SST29D2, the rainfall contributions of TFM and TFm are increased but the rainfall contributions of tFM and tFm are decreased. As a result, the rainfall contribution of the rainfall with water vapor convergence is barely changed. The increases of PRA for TFM and TFm are associated with the expanded rainfall coverage and enhanced surface rainfall through the increases in local atmospheric drying and rain hydrometeor loss/convergence in TFM and the slowdown in hydrometeor gain/divergence from rain and graupel clouds in TFm. The decrease of PRA for tFM results from the shrink of rainfall coverage. The rainfall contribution of TfM is enhanced when the diurnal variation of SST with the diurnal difference of 1°C is included in SST29D1 but it is barely changed as the diurnal difference increases from 1°C in SST29D1 to 2°C in SST29D2. The increase in rainfall contribution of TfM is associated with the expanded rainfall coverage and enhanced surface rainfall through the increases in local atmospheric drying and hydrometeor loss/convergence of water and graupel clouds.

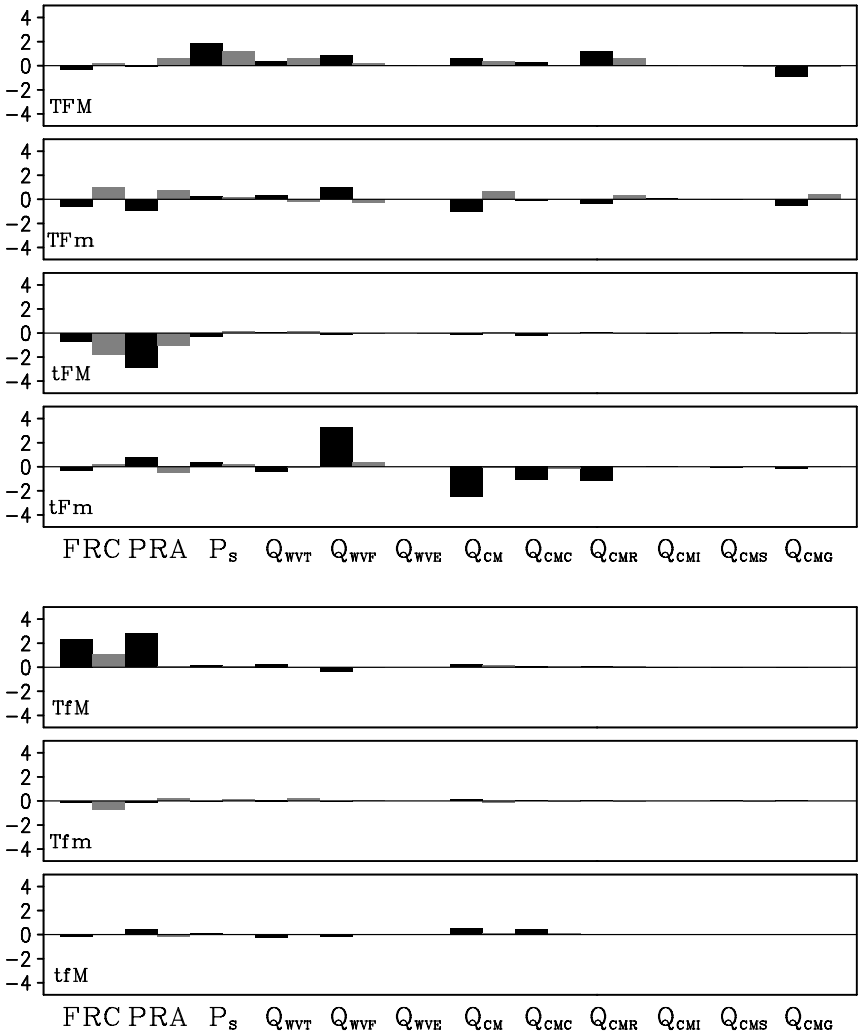

Figure 3. Fractional rainfall coverage (FRC) and percentage of rain amount over total rainfall amount (PRA), and means of P_S, Q_{WVT}, Q_{WVF}, Q_{WVE}, Q_{CM}, Q_{CMC}, Q_{CMR}, Q_{CMI}, Q_{CMS}, and Q_{CMG} of TFM, TFm, tFM, and tFm, TfM, Tfm, and tfM for SST29D1-SST29 (black) and SST29D2-SST29D1 (grey). Units are mm h^{-1} for P_S, Q_{WVT}, Q_{WVF}, Q_{WVE}, and Q_{CM} and % for FRC and PRA.

4 SUMMARY

The sensitivity of precipitation to sea surface temperature (SST) and its diurnal variation is investigated by analyzing the 10-day equilibrium model simulation data from a series of sensitivity experiments conducted by Gao et al.[6]. The experiments SST27, SST29, and SST31 are respectively imposed by the time-invariant SSTs of 27°C, 29°C, and 31°C. The experiments SST29D1

and SST29D2 are respectively forced by the diurnally varying SSTs with the time-mean of 29°C and diurnal amplitudes of 1°C and 2°C. All experiments are imposed by zero large-scale vertical velocity and time and height invariant large-scale zonal wind. The grid-scale rainfall simulation data are categorized into eight rainfall types based on different rainfall processes using the surface rainfall equation derived by Gao et al.[7]. The results are shown as follows:

(1) The largest contributor to total rainfall is the rainfall (TFm) with water vapor convergence and local atmospheric drying and hydrometeor gain/divergence in all of the experiments.

(2) The rainfall contribution by water vapor convergence is increased as the imposed time-invariant SST increases from 27°C to 29°C, and is decreased when the SST increases from 29°C to 31°C or the diurnal variation of SST with the diurnal difference of 1°C is imposed in the model. The rainfall contribution by water vapor convergence does not change as the diurnal difference of SST increases from 1°C to 2°C.

(3) The increase of SST from 27°C to 29°C primarily enhances the rainfall contribution of TFm by intensifying surface rainfall through the strengthened water vapor convergence, whereas the increase of SST from 29°C to 31°C primarily reduces the rainfall contribution of the rainfall (tFM) with water vapor convergence and local atmospheric moistening and hydrometeor loss/convergence and TFm through the shrink of rainfall coverage. The inclusion of diurnal variation of SST with the diurnal difference of 1°C in the model primarily reduces the rainfall contribution of tFM by reducing rainfall coverage and surface rainfall through the decreases in water vapor convergence and cloud water hydrometeor loss/convergence.

(4) Convective rainfall is usually associated with water vapor convergence. The comparison between this study and Zhou and Li[5] shows that the rainfall with water vapor convergence contributes more to total rainfall than convective rainfall does. This is consistent with the result in Shen et al.[8], in which the rainfall with water vapor convergence contributes 2.04% more to total rainfall than convective rainfall does, but the differences in this study are significantly larger than that in Shen et al.[8]. The increase of SST from 29°C to 31°C and the inclusion of diurnal variation of SST decrease the contribution of the rainfall with water vapor convergence whereas they increase the contribution of convective rainfall.

REFERENCES:

[1] LAU K M, SUI C H, TAO W K. A preliminary study of the tropical water cycle and its sensitivity to surface warming [J]. Bull. Amer. Meteor. Soc., 1993, 74: 1313-1321.

[2] COSTA A A, COTTON W R, WALKO R L, et al. SST Sensitivities in multi-day TOGA COARE cloud-resolving simulations [J]. J. Atmos. Sci., 2001, 58: 253-268.

[3] WU X, MONCRIEFF M W. Effects of sea surface temperature and large-scale dynamics on the thermodynamic equilibrium state and convection over the tropical western Pacific [J]. J. Geophys. Res., 1999, 104: 6093-6100.

[4] CUI X, LI X. Role of surface evaporation in surface rainfall processes [J]. J. Geophys. Res. 2006, 111, D17112, doi:10.1029/2005JD006876.

[5] ZHOU Y, LI X. Sensitivity of convective and stratiform rainfall to sea surface temperature [J]. Atmos. Res., 2009, 92: 212-219.

[6] GAO S, ZHOU Y, LI X. Effects of diurnal variations on tropical equilibrium states: A two-dimensional cloud-resolving modeling study [J]. J. Atmos. Sci., 2007, 64: 656-664.

[7] GAO S, CUI X, ZHOU Y, et al. Surface rainfall processes as simulated in a cloud resolving model [J]. J. Geophys. Res., 2005, 110, D10202, doi: 10.1029/2004JD005467.

[8] SHEN X, WANG Y, ZHANG N, et al. Precipitation and cloud statistics in the deep tropical convective regime [J]. J. Geophys. Res., 2010, 115, D24205, doi: 10.1029/2010JD014481.

[9] SOONG S T, OGURA Y. Response of tradewind cumuli to large-scale processes [J]. J. Atmos. Sci., 1980, 37: 2035-2050.

[10] SOONG S T, TAO W K. Response of deep tropical cumulus clouds to mesoscale processes [J]. J. Atmos. Sci., 1980, 37: 2016-2034.

[11] TAO W K, SIMPSON J. The Goddard Cumulus Ensemble model. Part I: Model description [J]. Terr. Atmos. Ocean. Sci., 1993, 4: 35-72.

[12] SUI C H, LAU K M, TAO W K, et al. The tropical water and energy cycles in a cumulus ensemble model [J]. Part I: Equilibrium climate [J]. J. Atmos. Sci., 1994, 51: 711-728.

[13] LI X, SUI C H, LAU K M, et al. Large-scale forcing and cloud-radiation interaction in the tropical deep convective regime [J]. J. Atmos. Sci., 1999, 56: 3028-3042.

[14] LIN Y L, FARLEY R D, ORVILLE H D, et al. Bulk parameterization of the snow field in a cloud model [J]. J. Climate Appl. Meteor., 1983, 22: 1065-1092.

[15] RUTLEDGE S A, HOBBS P V. The mesoscale and microscale structure and organization of clouds and precipitation in midlatitude cyclones. Part VIII: A model for the "seeder-feeder" process in warm-frontal rainbands [J]. J. Atmos. Sci., 1983, 40: 1185-1206.

[16] RUTLEDGE S A, HOBBS P V. The mesoscale and microscale structure and organization of clouds and precipitation in midlatitude cyclones. Part XII: A diagnostic modeling study of precipitation development in narrow cold-frontal rainbands [J]. J. Atmos. Sci., 1984, 41: 2949-2972.

[17] TAO W K, SIMPSON J, MCCUMBER M. An ice-water saturation adjustment [J]. Mon. Wea. Rev., 1989, 117, 231-235.

[18] KRUEGER S K, FU Q, LIOU K N, et al. Improvement of an ice-phase microphysics parameterization for use in numerical simulations of tropical convection [J]. J. Appl. Meteor., 1995, 34: 281-287.

[19] CHOU M D, KRATZ D P, RIDGWAY W. Infrared radiation parameterization in numerical climate models [J]. J. Climate, 1991, 4: 424-437.

[20] CHOU M D, SUAREZ M J, HO C H, et al.. Parameterizations for cloud overlapping and shortwave single scattering properties for use in general circulation and cloud ensemble models [J]. J. Atmos. Sci., 1998, 55: 201-214.

[21] GAO S, LI X. Cloud-resolving modeling of convective processes [M]. Berlin: Springer. 2008, 206pp.

[22] SUI C H, LAU K M. TAKAYABU Y, et al. Diurnal

variations in tropical oceanic cumulus ensemble during TOGA COARE [J]. J. Atmos. Sci., 1997, 54: 639-655.
[23] GAO S, PING F, LI X, et al. A convective vorticity vector associated with tropical convection: A two-dimensional cloud-resolving modeling study [J]. J. Geophys. Res., 2004, 109, D14106, doi:10.1029/2004JD004807.
[24] GAO S, CUI X, ZHOU Y, et al. A modeling study of moist and dynamic vorticity vectors associated with 2D tropical convection [J]. J. Geophys. Res., 2005, 110, D17104, doi:10.1029/2004JD005675.
[25] GAO S, RAN L, LI X. Impacts of ice microphysics on rainfall and thermodynamic processes in the tropical deep convective regime: A 2D cloud-resolving modeling study [J]. Mon. Wea. Rev., 2006, 134: 3015-3024.
[26] TAO W K, SIMPSON J, SUI C H, et al. Equilibrium states simulated by cloud-resolving models [J]. J. Atmos. Sci., 1999, 56: 3128-3139.
[27] TAO W K, SHIE C L, SIMPSON J, et al. Convective systems over the South China Sea: Cloud-resolving model simulations [J]. J. Atmos. Sci., 2003, 60: 2929-2956.
[28] TAO W K, JOHNSON D, SHIE C L, et al. The atmospheric energy budget and large-scale precipitation efficiency of convective systems during TOGA COARE, GATE, SCSMEX, and ARM: Cloud-resolving model simulations [J]. J. Atmos. Sci., 2004, 61: 2405-2423.
[29] LI X, SUI C H, LAU K M. Dominant cloud microphysical processes in a tropical oceanic convective system: A 2-D cloud resolving modeling study [J]. Mon. Wea. Rev. 2002, 130: 2481-2491.
[30] WANG D, LI X, TAO W K, et al. Torrential rainfall processes associated with a landfall of severe tropical storm Bilis (2006): A two-dimensional cloud-resolving modeling study [J]. Atmos. Res. 2009, 91: 94-104.
[31] WANG D, LI X, TAO W K, et al. Effects of vertical wind shear on convective development during a landfall of severe tropical storm Bilis (2006) [J]. Atmos. Res., 2009, 94: 270-275.
[32] WANG D, LI X, TAO W K. Responses of vertical structures in convective and stratiform regions to large-scale forcing during the landfall of severe tropical storm Bilis (2006) [J]. Adv. Atmos. Sci., 2010, 27: 33-46.
[33] WANG J J, LI X, CAREY L. Evolution, structure, cloud microphysical and surface rainfall processes of a monsoon convection during the South China Sea Monsoon Experiment [J]. J. Atmos. Sci., 2006, 64: 360-380.
[34] ZHOU Y, CUI X, LI X. Contribution of cloud condensate to Surface rain rate [J]. Prog. Nat. Sci., 2006, 16: 64-70.

Citation: ZHOU Yu-shu and Xiao-fan LI. Sensitivity of precipitation to sea surface temperature and its diurnal variation: A partitioning analysis based on surface rainfall budget. *J. Trop. Meteor.*, 2012, 18(3): 369-376.